JOURNAL OF CATALYSIS 77, 460–472 (1982)

Hydrogenation of CO_2 on Group VIII Metals

II. Kinetics and Mechanism of CO_2 Hydrogenation on Nickel

GORDON D. WEATHERBEE AND CALVIN H. BARTHOLOMEW[1]

BYU Catalysis Laboratory, Department of Chemical Engineering, Brigham Young University, Provo, Utah 84602

Received February 2, 1982; revised May 19, 1982

The rate of CO_2 hydrogenation on Ni/SiO_2 was measured as a function of H_2 and CO_2 partial pressures at 500–600 K, 140 kPa, and 30,000–90,000 h^{-1}. The data show that the rate of CO_2 hydrogenation is moderately dependent on CO_2 and H_2 concentrations at low partial pressures but essentially concentration independent at high partial pressures. Under most typical reaction conditions CO is observed as a product of the reaction at levels determined by quasi-equilibrium between surface and gas phase CO species. Addition of CO to the reactants above this equilibrium level causes a significant decrease in the rate of CO_2 hydrogenation apparently as a result of product inhibition. Reaction orders and the true activation energy are quite temperature dependent indicating that a simple power law rate expression provides an inadequate fit of the data. Indeed, the kinetic results are consistent with a complex Langmuir–Hinshelwood mechanism involving dissociative adsorption of CO_2 to CO and atomic oxygen followed by hydrogenation of CO via a carbon intermediate to methane.

INTRODUCTION

Hydrogenation of CO and CO_2 to methane on nickel catalysts are important reactions occurring in purification of ammonia feeds and methanation of coal-derived gas. CO_2 methanation is important in production of substitute natural gas, since it contributes additional methane (beyond that produced by CO methanation) needed to meet heating value specifications. Both reactions are also of interest in the production of process heat or power from reclaimable waste streams containing dilute carbon oxides or from nuclear reactor steam-reformed CO/H_2 streams as part of a so-called "heat pipeline."

Most of the previous research has emphasized the kinetics and mechanisms of CO methanation on nickel (*1–6*) while a few previous studies (*1, 2, 7–15*) have considered the kinetics and mechanisms of CO_2 on nickel. However, most of the early previous kinetic studies of CO_2 hydrogenation were conducted using poorly characterized catalysts under high conversion conditions so that the true kinetic behavior was masked by transport influences and/or catalyst deactivation, or they were carried out using a large excess of hydrogen so that the results were not applicable to most methanation processes.

On the basis of the early work, there have been a number of mechanisms proposed for CO_2 methanation. These fall generally into two categories: (i) conversion of CO_2 to CO via the reverse water gas shift reaction followed by CO methanation, and (ii) direct hydrogenation of CO_2 to methane by a mechanism distinct from CO methanation. Three recent studies (*16–18*) provide evidence that the first of these proposed mechanisms may be correct and that CO_2 methanation may proceed via CO_2 dissociation to CO and atomic oxygen (the latter of which is hydrogenated to H_2O) followed by further dissociation of CO to a carbon intermediate which is hydrogenated to methane.

[1] To whom correspondence should be addressed.

0021-9517/82/100460-13$02.00/0

In other words, following CO_2 adsorption and dissociation, CO_2 methanation apparently proceeds via the same route as CO methanation.

In a recent paper (*18*) we reported for the first time the specific activity for CO_2 methanation on well-characterized Ni/SiO_2. The results indicated the specific activity for CO_2 methanation on Ni to be the same within experimental error as that for CO methanation at 500–550 K, suggesting that CO and CO_2 methanation might occur through similar routes.

The purpose of this investigation was to obtain kinetic data over a range of temperatures, pressures, and reactant concentrations for the same well-characterized Ni/SiO_2 and to determine if these kinetics were consistent with any of the previously proposed mechanisms.

EXPERIMENTAL

A 3% Ni/SiO_2 catalyst was prepared by simple impregnation to incipient wetness of the support with an aqueous solution of nickel nitrate followed by oven drying at 375 K. The impregnated dried sample was reduced in H_2 while heating at 2 K/min to 750 K with a 2 h hold at 500 K and a 12 h hold at 750 K. A 0.3-g powdered sample of the catalyst (average particle diameter of 10^{-2} cm) was then passivated, transferred to a Pyrex cell, reduced, and evacuated 2 h each at 750 K and chemisorbed with H_2. From hydrogen chemisorption measurements at 298 K (*19*) the hydrogen uptake was found to be 100 μmol H_2/g catalyst, corresponding to a nickel dispersion of 30% assuming complete reduction to Ni metal (*19*). Further details concerning preparation and characterization of this catalyst were reported previously (*18*).

Hydrogen and nitrogen gases (99.99%) were purified by passing both through a palladium Deoxo purifier (Engelhard) and a dehydrated molecular sieve trap. Carbon monoxide (Matheson Purity, 99.99%) was purified by passing through a Molecular Sieve 5A trap. Carbon dioxide (Matheson Purity, 99.99%) was used without further purification.

Kinetic data for CO_2 methanation were obtained using 1 cm^3 (approx. 0.3 g) catalyst in an isothermal, tubular, 1 cm i.d., one-pass differential, stainless-steel reactor equipped with preheater and thermocouple in the catalyst bed. Tests were conducted at CO_2 conversions generally less than 10%, space velocities of 30,000–90,000 h^{-1}, total pressures between 140 and 175 kPa, and at 5 temperatures, 500, 525, 550, 575, and 600 K. The hydrogen partial pressure rate dependence was determined by holding the CO_2 partial pressure constant at 1% of the total pressure (approx. 1.38 kPa) and varying the H_2 pressure from 2.76 to 13.8 kPa (2–10% of total pressure). The CO_2 dependence was found in a similar manner with the H_2 pressure held constant at approximately 5.52 kPa (4% of total pressure) and CO_2 pressures varied from 0.276 to 2.76 kPa (0.2 to 2.0% of total pressure). The effect of rate inhibition by CO was found by holding the CO_2 and H_2 pressures constant at 1.38 and 5.62 kPa, respectively, and varying the CO pressure from 0 to 0.6 kPa (0.4% of total pressure). N_2 diluent was used to minimize heat and mass transfer effects and in all cases made up the remainder of the reactant gas. The kinetic data were fitted to various rate expressions by a nonlinear least squares routine.

RESULTS

Figure 1 shows the CH_4 turnover number for CO_2 methanation on 3% Ni/SiO_2 as a function of H_2 partial pressure at 525 K, 140 kPa total pressure, 1.40 kPa CO_2 partial pressure, and a space velocity of 30,000 h^{-1}. At low H_2 pressures the rate of CH_4 formation is moderately dependent on the H_2 concentration. The rate dependence on H_2 clearly diminishes with increasing H_2 pressure.

The CH_4 turnover number is shown as a function of CO_2 concentration in Fig. 2 at 525 K, 140 kPa total pressure, 5.60 kPa H_2 partial pressure, and a space velocity of

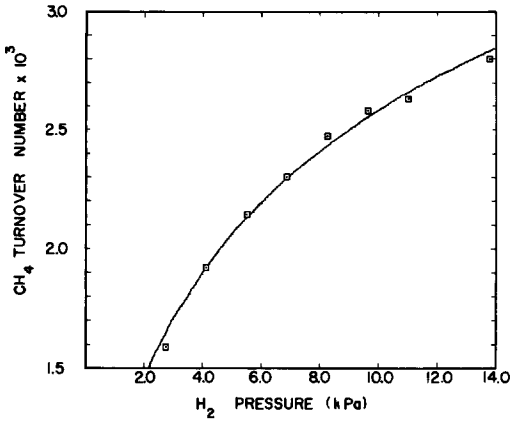

FIG. 1. Methane turnover number vs reactant H_2 partial pressure: 525 K, GHSV = 30,000 h^{-1}, 140 kPa total pressure, 1.4 kPa CO_2, balance N_2.

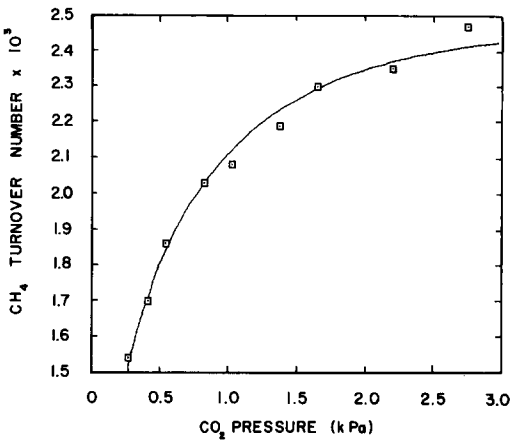

FIG. 2. Methane turnover number vs reactant CO_2 partial pressure: 525 K, GHSV = 30,000 h^{-1}, 140 kPa total pressure, 5.6 kPa H_2, balance N_2.

30,000 h^{-1}. As with H_2, the rate shows a moderately strong CO_2 pressure dependence at low CO_2 pressures and approaches zero-order dependence at higher CO_2 pressure.

Figure 3 shows the CH_4 turnover number for CO_2 methanation as a function of reactant CO concentration at 525 K, 30,000 h^{-1}, and 140 kPa total pressure (1% CO_2 and 4% H_2). The decreasing turnover number with increasing partial pressure of CO suggests a strong inhibition of methane production rate by adsorbed CO if present in the reactants at concentrations exceeding 0.017 kPa (0.012%). At each temperature an "equilibrium" CO concentration was observed in the products regardless of the level of CO present in the reactant mixture and independent of CO_2 conversion or space velocity. If the CO concentration in the reactant stream exceeded this equilibrium level, CO reacted preferentially over CO_2 to form CH_4, resulting in the inhibition of CO_2 methanation while at the same time decreasing the CO concentration in the direction of the equilibrium level.[2] Below the equilibrium CO concentration reactant CO had very little effect on the rate of CO_2 methanation (see Fig. 3). Table 1 lists the approximate CO equilibrium level found for each temperature studied.

The rate data were fitted to a simple power rate law expression of the form:

$$r_{CH_4} = k_0 P_{H_2}{}^x P_{CO}{}^y. \quad (1)$$

An Arrhenius plot of k_0 in Fig. 4 shows that the "apparent" activation energy shifts from about 89 kJ/mol at low temperatures to 39 kJ/mol at higher temperatures.

Figures 5 and 6 show the apparent H_2 and CO_2 reaction orders for a power law fit of the data as a function of temperature. The CO_2 order can be seen to drop steadily with temperature while the H_2 order increases with temperature.

A Langmuir–Hinshelwood rate expression (see derivation in the Appendix) was also fitted to the rate data. The solid lines in Figs. 1, 2, and 3 show a nonlinear least-squares fit of this rate equation to the experimental data. Table 2 lists the rate expression and the kinetic and adsorption equilibrium constants k_4, K_2, and K_3 for each temperature tested. The activation energy for k_4 was found to be 94 kJ/mol (see

[2] At lower temperatures the constant outlet or "equilibrium" CO concentration was observed over a broad range of CO concentrations relative to the "equilibrium" concentration, whereas at high temperatures a constant outlet CO concentration was observed only if the inlet CO concentration was near that of the "equilibrium level."

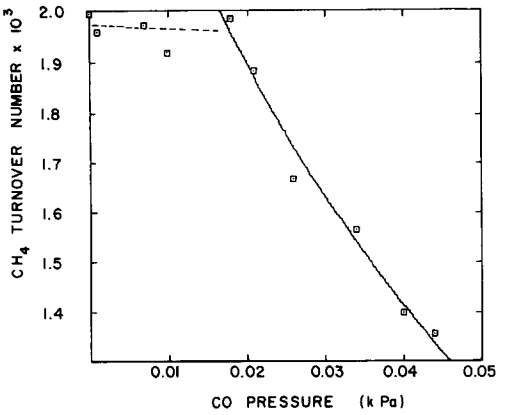

FIG. 3. Methane turnover number vs reactant CO partial pressure: 525 K, GHSV = 30,000 h^{-1}, 140 kPa total pressure, 5.6 kPa H_2, 1.4 kPa CO_2, balance N_2.

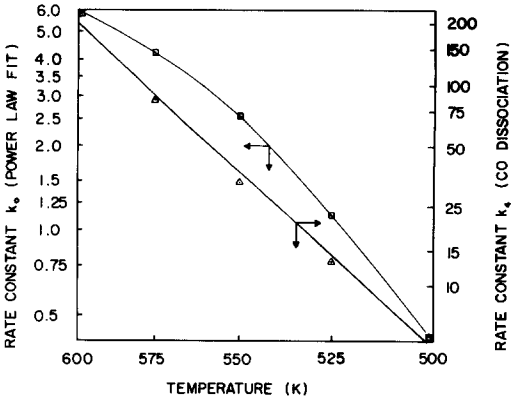

FIG. 4. Arrhenius plots of rate constants. □, k_0, rate constant from power law fit; △, k_4, rate constant for CO dissociation.

Fig. 4). It was not possible to determine independent values of the other rate constants (besides k_4) and adsorption equilibrium constants (besides K_2 and K_3) in Table 2; hence values are reported for groupings of these constants.

DISCUSSION

Comparison of Kinetic Data with Those from Previous Studies

Previously reported rate expressions for CO_2 hydrogenation are listed in Table 3 and compared with the rate equation for CO_2 methanation from this study. Only those studies performed in the absence of heat and mass transport influences (*12–15*) provide intrinsic kinetic and mechanistic information. Three of these studies (*12–14*) were performed using low CO_2 concentrations in a large excess of H_2 and thus provide information on the CO_2 concentration dependence only. For example Herwijnen *et al.* (*14*) observed a first-order CO_2 dependency at CO_2 partial pressures below 0.004 atm changing to zero-order dependency above 0.015 atm. The Czechoslovakian workers (*12, 13*) reported the rate to be 0.5 order in CO_2. In a very recent study of CO_2 methanation on Raney nickel, Lee and Anderson (*15*) found positive orders for both CO_2 and H_2 at low concentrations, both changing to zero-order at high concentrations. The re-

TABLE 1

CO Equilibrium Levels[a] in CO_2 Hydrogenation, 140–175 kPa, 4% H_2, 1% CO_2, 30,000–90,000 h^{-1}

Temperature (K)	% CO at equilibrium
500	0.003
525	0.012
550	0.028
575	0.078
600	0.120

[a] Observed at the reactor outlet for a fixed temperature and gas composition independent of space velocity, conversion, and inlet CO concentration.

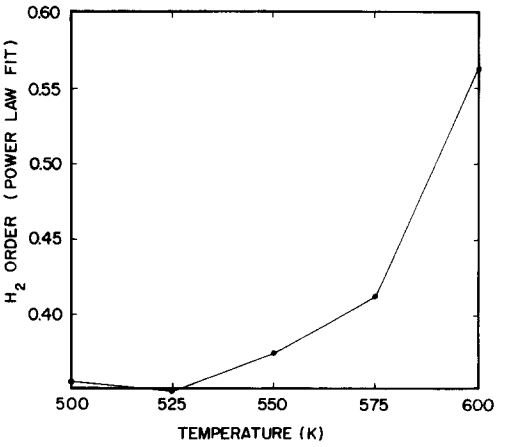

FIG. 5. H_2 order in power law rate equation vs temperature. GHSV = 30,000–90,000 h^{-1}, 140–175 kPa, 95% N_2, 4% H_2, 1% CO_2.

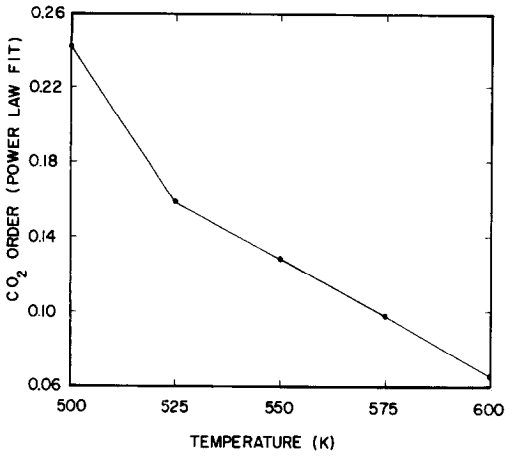

FIG. 6. CO_2 order in power law rate equation vs temperature. GHSV = 30,000–90,000 h^{-1}, 140–175 kPa, 95% N_2, 4% H_2, 1% CO_2.

action order trends of this study show excellent agreement with those of Lee and Anderson and are consistent with the earlier results (*12–14*).

Our activation energy of 94 kJ/mol is in good agreement with the value of 105.8 reported by Herwijnen *et al.* However, our study is the first to show that reaction orders and activation energies based on a power law expressions shift significantly with temperature (see Figs. 4–6). In other words, the simple power law model is inadequate in describing the kinetics. The changing activation energy of the rate constant in the power law fit with temperature easily explains the large variation of activation energies reported in the literature, since previous studies were carried out in different ranges of temperature.

Kinetics and Mechanisms of CO_2 Hydrogenation

There has been considerable controversy in the literature regarding the mechanism of CO_2 hydrogenation, i.e., whether it proceeds by transformation of CO_2 to CO followed by CO hydrogenation or by a unique set of elementary steps. A mechanism for CO_2 hydrogenation which accounts for the observations of this and other recent studies (*15–18, 20–27*) is summarized in Table 4.

This mechanism assumes that H_2 and CO_2 adsorption occur dissociatively to hydrogen atoms, CO, and oxygen atoms. Adsorbed CO can dissociate further to carbon and oxygen atoms or desorb. Further steps include hydrogenation of the adsorbed carbon and carbene intermediates to methane and of atomic oxygen to water.

TABLE 2

Values of Kinetic Constants from a Langmuir–Hinshelwood[a] Fit of the Data

Temperature (K)	$\left(\frac{K_1K_2K_{10}k_4K_{11}}{2}\right)^{1/2}$	$\left(\frac{2K_2k_4}{K_1K_{10}k_{11}}\right)^{1/2}$	$\left(\frac{K_1K_2K_{10}k_{11}}{2k_4}\right)^{1/2}$	$\left(\frac{1}{K_3}\right)$	K_2	k_4	$\frac{\Sigma \text{ err}^2}{(\bar{n})^2}$[b]
500	0.535	0.156	0.0997	22.8	0.016	5.37	0.0106
525	1.86	0.289	0.140	8.24	0.040	13.3	0.00732
550	4.73	0.419	0.143	1.99	0.060	33.1	0.00740
575	8.05	0.704	0.0936	1.38	0.066	86.0	0.00125
600	15.9	0.998	0.0678	0.909	0.068	235.	0.00429

[a] $$r = \frac{\left(\frac{K_1K_2K_{10}k_4k_{11}}{2}\right)^{1/2} L^2 P_{CO_2}^{1/2} P_{H_2}^{1/2}}{\left(1 + \left(\frac{2K_2k_4}{K_1K_{10}k_{11}}\right)^{1/2} \frac{P_{CO_2}^{1/2}}{P_{H_2}^{1/2}} + \left(\frac{K_1K_2K_{10}k_{11}}{2k_4}\right)^{1/2} P_{CO_2}^{1/2} P_{H_2}^{1/2} + \frac{P_{CO}}{K_3}\right)^2}$$

where L = the total number of available surface sites; L is normalized to the total number of surface sites determined by H_2 adsorption and hence has a value of unity in the above expression. r has units of molecules of methane produced per site per second.

[b] $\bar{n}$ = average rate; Σ err^2 = sum of the errors squared from the least-squares fit.

TABLE 3

Rate Equations and Activation Energies Reported for CO_2 Hydrogenation on Nickel

Rate equations	E_{act} (kJ/mol)	Reference
$r = \frac{C_1 P_{CO_2} P_{H_2}^4}{(P_{H_2}^{1/2} + C_{P_{CO_2}} + C_3)}$	—	(*7, 8*)
$r = \frac{K P_{CO_2} P_{H_2}^4}{(1 + K_1 P_{H_2} + K_2 P_{CO_2})^5}$	54.8–58.1	(*9, 10*)
$r = \frac{aBP_T}{1 + BP_T}$	54.8	(*13*)
$r = kC_{CO_2}^{0.5}$	85.7	(*12, 13*)
$r = kP_{CO_2}$	54.3	(*1*)
$r_{CO_2} = \frac{1.36 \times 10^{12} \exp(-105{,}800/RT) P_{CO_2}}{(1 + 1270 P_{CO_2})}$ (mole hr^{-1} g^{-1})	105.8	(*14*)
$r_{CH_4} = \frac{\left(\frac{K_1 K_2 K_{10} k_4 k_{11}}{2}\right)^{1/2} L^2 P_{CO_2}^{1/2} P_{H_2}^{1/2}}{\left(1 + \left(\frac{2K_2 k_4}{K_1 K_{10} k_{11}}\right)^{1/2} \frac{P_{CO_2}^{1/2}}{P_{H_2}^{1/2}} + \left(\frac{K_1 K_2 K_{10} k_{11}}{2k_4}\right)^{1/2} P_{CO_2}^{1/2} P_{H_2}^{1/2} + \frac{P_{CO}}{K_3}\right)^2}$ where E_4 = 94 kJ/mol		(This study)

Evidence in support of this mechanism can be summarized as follows. Several previous studies (*16, 17, 22, 24*) have established that CO_2 adsorbs dissociatively on nickel especially at temperatures above 298 K, although it is generally adsorbed in smaller quantities than is CO and is easily displaced by CO at room temperature (*16*). In a very recent temperature-programmed desorption study Falconer and Zagli (*17*) found dissociative CO_2 adsorption to be activated above room temperature reaching a maximum at 473 K. Upon reacting H_2 with CO_2 that had been preadsorbed at elevated temperatures they found a peak at room temperature corresponding to reaction of H_2 and atomic oxygen to water. Above room temperature the temperature-programmed reaction spectrum following CO_2 adsorption was the same as the spectrum following CO adsorption, suggesting that both CO and CO_2 methanation proceed via the same rate-determining step, namely, CO dissociation. If this is true then the rates of CO and CO_2 methanation should be the same under conditions where the rate-determining steps are the same for both reactions. Indeed, the results of our previous study confirm that the rates are the same for both reactions at low temperature (*18*).

Falconer and Zagli (*17*) observed that adsorbed CO_2 desorbed as both CO_2 and CO at higher temperatures consistent with the observation in this and previous studies (*18, 20*) that CO is a product of CO_2 methanation. Thus, Reaction 3 accounts for the occurrence of CO in the gas phase as well as the product inhibition by CO (*1, 2, 14, 15, 18*). The fact that in this study and in our previous study (*18*) a constant CO product concentration was observed at a fixed temperature, pressure, and gas composition independent of space velocity or conversion suggests that adsorbed CO is in equilibrium with gas phase CO. This is also suggested by the equilibrium CO levels obtained in the CO inhibition tests conducted in this study.

TABLE 4

Proposed Sequence of Elementary Steps in CO_2 Methanation[a]

Reaction	Equation
$H_2(g) + 2\,S \underset{k_{-1}}{\overset{k_1}{\rightleftharpoons}} 2\,H\text{–}S$	(4-1)
$CO_2(g) + 2\,S \underset{k_{-2}}{\overset{k_2}{\rightleftharpoons}} CO\text{–}S + O\text{–}S$	(4-2)
$CO\text{–}S \underset{k_{-3}}{\overset{k_3}{\rightleftharpoons}} CO(g) + S$	(4-3)
$CO\text{–}S + S \underset{k_{-4}}{\overset{k_4}{\rightleftharpoons}} C\text{–}S + O\text{–}S$	(4-4)
$C\text{–}S + H\text{–}S \underset{k_{-5}}{\overset{k_5}{\rightleftharpoons}} CH\text{–}S + S$	(4-5)
$CH\text{–}S + H\text{–}S \underset{k_{-6}}{\overset{k_6}{\rightleftharpoons}} CH_2\text{–}S + S$	(4-6)
$CH_2\text{–}S + H\text{–}S \underset{k_{-7}}{\overset{k_7}{\rightleftharpoons}} CH_3\text{–}S + S$	(4-7)
$CH_3\text{–}S + H\text{–}S \underset{k_{-8}}{\overset{k_8}{\rightleftharpoons}} CH_4\text{–}S + S$	(4-8)
$CH_4\text{–}S \underset{k_{-9}}{\overset{k_9}{\rightleftharpoons}} CH_4(g) + S$	(4-9)
$O\text{–}S + H\text{–}S \underset{k_{-10}}{\overset{k_{10}}{\rightleftharpoons}} OH\text{–}S + S$	(4-10)
$OH\text{–}S + H\text{–}S \underset{k_{-11}}{\overset{k_{11}}{\rightleftharpoons}} H_2O\text{–}S + S$	(4-11)
$H_2O\text{–}S \underset{k_{-12}}{\overset{k_{12}}{\rightleftharpoons}} H_2O(g) + S$	(4-12)

[a] S refers to a surface site.

Based on the mechanism in Table 4, it was possible, depending upon the assumptions made, to derive many different Langmuir–Hinshelwood expressions. Over 30 different expressions were derived and checked against the data using a least-squares routine. The physical validity of the derived constants was also checked for each expression. Examples of expressions based on different rate determining steps are listed in Table 5.

Assuming CO_2 adsorption to be the rate-determining step produces Eq. (5-1). This equation predicts the H_2 order to be negative in all cases, contrary to the experimental results shown in Fig. 5.

The assumption that H_2 chemisorption is the rate-determining step produces Eq. (5-2). Examination of this equation shows that it does not fit the data, since it predicts first order in H_2 and negative order in CO_2.

A number of expressions resulted from assuming CO dissociation (Eq. (4.4) in Table 4) to be rate limiting. In most of these derivations, Steps 1, 2, 3, and 10 were assumed to be in quasi-equilibrium, while the surface oxygen concentration was found from the steady-state approximation. Depending upon the choice of the most abundant surface intermediates, several different rate equations were possible, two of which are shown in Table 5. Several of these expressions (Eq. (5-3) included) were eliminated because the least-squares fit of the data resulted in negative kinetic and/or equilibrium constants at all temperatures. Several other equations were rejected on the basis of a poor fit to the data. Equation (5-4) (see derivation in the Appendix) was found to provide an excellent fit to the data, as seen in Figs. 1, 2, and 3. Moreover, it was the only rate expression that resulted in physically meaningful rate and adsorption equilibrium constants as well as a linear Arrhenius plot (see Table 2 and Fig. 4) for the rate constant k_4. Values of k_4 calculated from other equations developed with CO dissociation as the rate-limiting step were not reasonable in that the activation energy approached infinity. In some cases it was not possible to isolate k_4 so that it could be calculated.

Assuming hydrogenation of C–S or CH–S (steps 5 and 6 in Table 4) to be the rate-determining step resulted in rate expressions similar in form to those for CO dissociation as the rate-determining step (see Table 5). In their derivation Steps 1, 2, 3, 4, and 10 were assumed to be in quasi-equilibrium. Step 5 was also assumed to be at equilibrium in the latter case. Again, the surface oxygen concentration was found from the steady-state approximation. A number of different rate expressions were derived for different assumptions regarding

TABLE 5

Kinetic Rate Expressions for CO_2 Methanation Based on Langmuir–Hinshelwood Kinetics

RDS[a]: CO_2 adsorption
MASI[b]: H–S[c]

$$r = \frac{k_2 L^2 P_{CO_2}}{(1 + K_1^{1/2} P_{H_2}^{1/2})^2} \tag{5-1}$$

RDS: H_2 adsorption
MASI: Dissociatively adsorbed CO_2

$$r = \frac{k_1 L^2 P_{H_2}}{(1 + K_2^{1/2} P_{CO_2}^{1/2})^2} \tag{5-2}$$

RDS: CO dissociation
MASI: H–S, CO–S
Assumptions: Steps 1, 2, 3, 10 (Table 4) in "quasi-equilibrium"

$$r = \frac{\left(\frac{K_1 K_2 K_{10} k_4 k_{11}}{2}\right)^{1/2} L^2 P_{CO_2}^{1/2} P_{H_2}^{1/2}}{\left(1 + K_1^{1/2} P_{H_2}^{1/2} + \left(\frac{K_1 K_2 K_{10} k_{11}}{2k_4}\right)^{1/2} P_{CO_2}^{1/2} P_{H_2}^{1/2} + \frac{P_{CO}}{K_3}\right)^2} \tag{5-3}$$

RDS: CO dissociation
MASI: O–S, CO–S
Assumptions: Steps 1, 2, 3, 10 in "quasi-equilibrium" (see Appendix for derivation)

$$r = \frac{\left(\frac{K_1 K_2 K_{10} k_4 k_{11}}{2}\right)^{1/2} L^2 P_{CO_2}^{1/2} P_{H_2}^{1/2}}{\left(1 + \left(\frac{2K_2 k_4}{K_1 K_{10} k_{11}}\right)^{1/2} \frac{P_{CO_2}^{1/2}}{P_{H_2}^{1/2}} + \left(\frac{K_1 K_2 K_{10} k_{11}}{2k_4}\right)^{1/2} P_{CO_2}^{1/2} P_{H_2}^{1/2} + \frac{P_{CO}}{K_3}\right)^2} \tag{5-4}$$

RDS: C hydrogenation
MASI: H–S, C–S, CO–S
Assumptions: Steps 1, 2, 3, 4, 10 in "quasi-equilibrium"

$$r = \frac{\left(\frac{K_2 K_4 K_{10}^2 k_5 k_{11}^2}{4}\right)^{1/3} K_1^{5/6} L^2 P_{CO_2}^{1/3} P_{H_2}^{5/6}}{\left(1 + K_1^{1/2} P_{H_2}^{1/2} + \left(\frac{K_2 K_4 K_{10}^2 k_{11}^2}{4k_5^2 K_1}\right)^{1/3} P_{CO_2}^{1/3} P_{H_2}^{1/3} + \frac{P_{CO}}{K_3}\right)^2} \tag{5-5}$$

RDS: CH hydrogenation
MASI: CH–S, H–S, CO–S
Assumptions: Steps 1, 2, 3, 4, 5, 10 in "quasi-equilibrium"

$$r = \frac{\left(\frac{K_2 K_4 K_5 K_{10} k_6 k_{11}^2}{4}\right)^{1/3} K_1 L^2 P_{CO_2}^{1/3} P_{H_2}}{\left(1 + K_1^{1/2} P_{H_2}^{1/2} + \left(\frac{K_1^{3/2} K_2 K_4 K_5 k_{11}^2}{4k_6^2}\right)^{1/3} P_{CO_2}^{1/3} P_{H_2}^{1/2} + \frac{P_{CO}}{K_3}\right)^2} \tag{5-6}$$

[a] RDS, rate-determining step.
[b] MASI, most abundant surface intermediates.
[c] L, total concentration of surface sites.

the most abundant surface intermediates. The least-squares fit of the data eliminated several of the possible equations in that they give negative constants over the whole temperature range. Two of the most plausible remaining expressions are listed in Table 5, one possible equation each for C hydrogenation and CH hydrogenation as the

rate-determining steps. Further calculation of rate constants for C hydrogenation and for CH hydrogenation eliminated Eqs. (5-5) and (5-6) from consideration, as the calculated activation energies for k_5 and k_6 were found to approach infinity in the temperature range 500–600 K.

Thus, the computer fitting of the experimental data to a large number of possible rate equations along with consideration of the physical validity of the derived rate expressions showed Eq. (5-4) to be most consistent with the data and to provide physically meaningful rate parameters. Indeed, the activation energy of 94 kJ/mol is consistent with values reported previously for the dissociation of CO (*27–29*). Although the calculated values for K_2, the "adsorption equilibrium constant" for Step 2, show a temperature dependence opposite of that expected for adsorption of CO_2 on clean single crystal nickel surfaces (*30–32*), this does not imply that Eq. (5-4) is invalid. In general, values for an adsorption equilibrium constant such as $1/K_3$, the adsorption equilibrium constant for CO (Table 2), are expected to decrease with temperature; however, values for K_2, the adsorption equilibrium constant for CO_2, increase with temperature. Nevertheless, Carberry (*31*) and Satterfield (*32*) point out that the adsorption equilibrium constants found from Langmuir–Hinshelwood rate equations may bear little relationship to those found directly in chemisorption equilibrium studies because of the loose assumptions made in deriving the Langmuir isotherm. Thus positive "adsorption heats" are not ruled out (*31, 32*). In addition the presence of other adsorbed intermediate reaction species such as carbon, oxygen, or hydrogen can exert a significant influence on the adsorption of a given species (*6, 30–33*), changing the observed nature of the equilibrium adsorption thermodynamics, even allowing for the possibility of negative equilibrium constants in the case of enhanced adsorption (*33*). Finally it should be noted that steady-state phenomena other than surface reactions (e.g., contributions from adsorption, desorption, surface diffusion, and readsorption processes) and reaction rates on nonideal surfaces may fit the Langmuir–Hinshelwood form. Thus, the heats of adsorption derived from Langmuir–Hinshelwood kinetic models are not likely to be of great significance so long as complex reactions on partially covered nonideal surfaces are involved (*31*).

It is interesting that the Arrhenius plot for k_0 (power law fit) shows a shift at higher temperatures while that for k_4 (Eq. (5-4)) is linear over the same range of temperature (see Fig. 4). The shift in apparent activation energy for k_0, the rate constant for a power law fit, might indicate a possible shift in the rate-determining step for the reaction. However, in view of the fact that the plot for k_4 is reasonably linear, the shift in E_0 may be due to the combination of kinetic and adsorption coefficients which increase and/or decrease with temperature. Indeed, the complex combination of constants in the denominator of Eq. (5-4) provides the basis for explaining this shift.

Evidence that hydrogenation of carbon (Step 5) may be the principal rate-determining step in CO methanation at least under selected reaction conditions has been provided by a number of recent studies (*5, 6, 23–27, 34*). The proposal from this study that CO dissociation is the rate-limiting step in CO_2 hydrogenation does not necessarily contradict this conclusion. Indeed, a recent kinetic study of CO methanation in this laboratory (*6*) provides evidence that there are several mechanistic regimes involving different rate-controlling steps whose importance depends mainly on temperature. At moderate reaction temperatures (525–575 K), CO dissociation appears to be rate-controlling while hydrogenation of carbon apparently controls at higher reaction temperatures (>575 K). This suggests that CO and CO_2 methanation rates on nickel are both controlled by CO dissociation at moderate reaction temperatures (525–575 K), a hypothesis consistent with

the observation of nearly identical specific reaction rates in CO_2 and CO methanation on Ni/SiO_2 in this temperature regime (*18*). Furthermore, it is possible for the two (CO and CO_2 hydrogenation) reactions to follow similar paths and still have different rate-determining steps. As a result of CO_2 dissociation higher levels of oxygen can be expected on the catalyst surface in CO_2 hydrogenation compared to CO hydrogenation. Indeed, lower surface coverages of CO and higher coverages of oxygen have been observed in TPD studies (*17, 24*). These higher levels of surface oxygen could very well alter the rate of CO dissociation in CO_2 methanation relative to those in CO methanation. Therefore it is not unreasonable to expect CO dissociation to be the rate-determining step in CO_2 hydrogenation even under conditions where the rate of CO hydrogenation is controlled by hydrogenation of carbon.

Nevertheless, further work in addition to kinetic studies will be needed to confirm this hypothesis. Moreover, the possibility that other steps may be rate determining is not ruled out by this study. That is, while the careful examination of a large number of rate expressions led to the choice of Eq. (5-4) as the most plausible and reasonable fit of the data, it should be emphasized that this does not prove that the assumptions made in deriving this rate expression are correct nor does it preclude the possible discovery of other rate expressions based on the proposed mechanism or other mechanisms which may fit the data equally well.

In some of the previous literature (*1, 2*) it was suggested that a few ppm CO could significantly inhibit the methanation of CO_2. The data from this study indicate that the degree to which CO inhibits the rate of CO_2 methanation varies with temperature (see Table 1). Thus at 500 K, a concentration of only 30 ppm is sufficient to significantly retard the reaction, while at 600 K, CO concentrations greater than 0.12% (1200 ppm) are necessary to cause inhibition. Thus the inhibiting effect of CO becomes progressively less with increasing temperatures. Moreover, it would diminish with increasing diffusional resistance for CO methanation at high conversions. Hence, the inhibition by CO would be greatly diminished in large industrial reactors where high CO conversions and/or high temperatures can occur either inside catalyst particles or along the axial length of the reactor.

Our previous study (*18*) of hydrogenation of CO_2 on nickel showed that a much lower fraction of higher molecular weight hydrocarbons is formed in CO_2 hydrogenation than in CO hydrogenation. Dalmon and Martin (*16*) explained this by suggesting that the additional adsorbed oxygen from CO_2 dissociation interferes with the formation of C–C bonds. Falconer and Zagli (*17*) suggested that CO_2 adsorption is slower and weaker than CO adsorption and thus results in higher H_2 to CO ratios on the catalyst surface which in turn favor methane formation. The proposed kinetic model in this study is consistent with these views. That is, if the dissociation of CO is rate limiting in CO_2 hydrogenation, the level of carbon on the surface should be much less than the level of carbon on the surface during CO hydrogenation where CO dissociates rapidly to give carbon. As a result higher hydrogen to carbon ratios should be expected in CO_2 hydrogenation, thus giving a much higher selectivity to hydrogen-rich products such as methane. Moreover, the fact that positive orders are observed for CO_2 in CO_2 methanation while negative orders are observed for CO in CO methanation (*6*) is indeed consistent with the view that CO_2 is more weakly adsorbed than CO.

CONCLUSIONS

(1) The kinetic data from this study show that the rate of CO_2 hydrogenation on Ni/SiO_2 is quite sensitive to reactant concentrations at low H_2 and CO_2 partial pressures while reaction orders approach zero for H_2 and CO_2 at high reactant concentrations.

Reaction orders for H_2 and CO_2 also vary with temperature. Accordingly, a simple power rate law is inadequate to describe the kinetics of the reaction. Nevertheless, the data are fitted well by a Langmuir–Hinshelwood rate expression.

(2) From the power law fit of the data the apparent activation energy for CO_2 hydrogenation on Ni/SiO_2 decreases from 89 to 39 kcal/mol as temperature is increased from 500 to 600 K. However, the activation energy for CO dissociation determined from the temperature dependence of the Langmuir–Hinshelwood reaction rate constant is constant at 94 kJ/mol over the full range of temperature (500–600 K).

(3) The observed kinetics from this investigation are consistent with a mechanism involving dissociative adsorption of CO_2 to CO and atomic oxygen followed by dissociation of adsorbed CO to atomic carbon and atomic oxygen. Methane is then formed by the hydrogenation of atomic carbon. In other words, the data favor a reaction sequence which proceeds via CO hydrogenation. This mechanism accounts for several unique aspects of CO_2 hydrogenation including the high selectivity to methane and the inhibition by CO.

APPENDIX

Derivation of Rate Expression 5.4

1. Step 4, dissociation of adsorbed CO, is assumed to be rate determining.

$$\frac{d(CH_4)}{dt} = k_4(CO\text{–}S)(S) \qquad \text{(A-1)}$$

2. Determination of (H–S): Step 1, dissociative adsorption of H_2, is assumed to be in quasi-equilibrium.

$$k_1 P_{H_2}(S)^2 = k_1(H\text{–}S)^2$$
$$(H\text{–}S) = K_1^{1/2} P_{H_2}^{1/2}(S). \qquad \text{(A-2)}$$

3. Determination of (O–S): From the steady state approximation:

$$\frac{d(O\text{–}S)}{dt} = 0 = k_2 P_{CO_2}(S)^2 - k_{-2}(CO\text{–}S)(O\text{–}S) + k_4(CO\text{–}S)(S) - k_{10}(O\text{–}S)(H\text{–}S) + k_{-10}(OH\text{–}S)(S). \qquad \text{(A-3)}$$

At steady state the net rate of production of (O–S) from Step 2 is equal to the net rate of (CO–S) production, which is approximately equal to the rate of CH_4 production. The production of CO(g) from Step 3 is assumed to be small; hence

$$r_2 \approx r_4$$
$$k_2 P_{CO_2}(S)^2 - k_{-2}(CO\text{–}S)(O\text{–}S) \approx k_4(CO\text{–}S)(S). \qquad \text{(A-4)}$$

Net rate of Step 10:

$$r_{10} = k_{10}(O\text{–}S)(H\text{–}S) - k_{-10}(OH\text{–}S)(S). \qquad \text{(A-5)}$$

Net rate of Step 11: H_2O (g) concentration is assumed to be small at low conversions. Steps 11 and 12 are assumed to be shifted far to the right such that $k_{-11}(S)(H_2O\text{–}S) \ll k_{11}(OH\text{–}S)(H\text{–}S)$. Therefore:

$$r_{11} = k_{11}(OH\text{–}S)(H\text{–}S). \qquad \text{(A-6)}$$

At steady state Steps 10 and 11 must proceed at the same rate,

$$r_{10} = r_{11} \qquad \text{(A-7)}$$
$$k_{10}(O\text{–}S)(H\text{–}S) - k_{-10}(OH\text{–}S)(S) = k_{11}(OH\text{–}S)(H\text{–}S). \qquad \text{(A-8)}$$

Substitute (A-4) and (A-8) into (A-3)

$$0 \approx k_4(CO\text{–}S)(S) + k_4(CO\text{–}S)(S) - k_{11}(OH\text{–}S)(H\text{–}S). \qquad \text{(A-9)}$$

The forward and reverse rates of Steps 10 are assumed to be large compared to the net rate of Step 10, i.e., Step 10 is near quasi-equilibrium. This fact enables an approximate solution for (OH–S):

$$k_{10}(O\text{–}S)(H\text{–}S) \approx k_{-10}(OH\text{–}S)(S)$$
$$(OH\text{–}S) \approx \frac{K_{10}(O\text{–}S)(H\text{–}S)}{(S)}. \qquad \text{(A-10)}$$

Substitute (A-10) into (A-9) to eliminate (OH–S):

$$0 \approx 2k_4(\text{CO–S})(\text{S}) - \frac{K_{10}k_{11}(\text{O–S})(\text{H–S})^2}{(\text{S})}$$

$$(\text{O–S}) = \frac{2k_4(\text{CO–S})(\text{S})^2}{K_{10}k_{11}(\text{H–S})^2}. \quad \text{(A-11)}$$

Substitute (A-2) into (A-11):

$$(\text{O–S}) = \frac{2k_4(\text{CO–S})}{K_1K_{10}k_{11}P_{\text{H}_2}}. \quad \text{(A-12)}$$

4. Determination of (CO–S): Step 2, dissociative adsorption of CO_2, is assumed to be in quasi-equilibrium.

$$k_2P_{\text{CO}_2}(\text{S})^2 \approx k_2(\text{CO–S})(\text{O–S})$$

$$(\text{CO–S}) \approx \frac{K_2P_{\text{CO}_2}(\text{S})^2}{(\text{O–S})}. \quad \text{(A-13)}$$

Substitute (A-12) into (A-13) while solving for (CO–S)

$$(\text{CO–S}) = \left(\frac{K_1K_2K_{10}k_{11}}{2k_4}\right)^{1/2} P_{\text{CO}_2}{}^{1/2}P_{\text{H}_2}{}^{1/2}(\text{S}). \quad \text{(A-14)}$$

Step 3 is assumed to be in quasi-equilibrium

$$k_3(\text{CO–S}) = k_{-3}P_{\text{CO}}(\text{S})$$

$$(\text{CO–S}) = \frac{P_{\text{CO}}(\text{S})}{K_3}. \quad \text{(A-15)}$$

Substitute (A-14) into (A-12) while solving for (O–S)

$$(\text{O–S}) = \left(\frac{2K_2k_4}{K_1K_{10}k_{11}}\right)^{1/2} \frac{P_{\text{CO}_2}{}^{1/2}}{P_{\text{H}_2}{}^{1/2}}(\text{S}). \quad \text{(A-16)}$$

5. Determination of (S): Since O–S and CO–S are assumed to be the most abundant surface intermediates (MASI), the total concentration of surface sites L is approximately:

$$L = (\text{S}) + (\text{O–S}) + (\text{CO–S}). \quad \text{(A-17)}$$

(CO–S) arises from two sources: (i) Step 2, the dissociation of CO_2 and (ii) adsorption of CO(g) in Step 3. Both sources must be accounted for in (A-17). Substitute (A-14), (A-15), and (A-16) into (A-17) while solving for S:

$$(\text{S}) = \frac{L}{\left(1 + \left(\frac{2K_2k_4}{K_1K_{10}k_{11}}\right)^{1/2} \frac{P_{\text{CO}_2}{}^{1/2}}{P_{\text{H}_2}{}^{1/2}} + \left(\frac{K_1K_2K_{10}k_{11}}{2k_4}\right)^{1/2} P_{\text{CO}_2}{}^{1/2}P_{\text{H}_2}{}^{1/2} + \frac{P_{\text{CO}}}{K_3}\right)}. \quad \text{(A-18)}$$

6. Final Substitution: Substitute (A-14) and (A-18) into (A-1):

$$\frac{d(\text{CH}_4)}{dt} = \frac{\left(\frac{K_1K_2K_{10}k_4k_{11}}{2}\right)^{1/2} L^2P_{\text{CO}_2}{}^{1/2}P_{\text{H}_2}{}^{1/2}}{\left(1 + \left(\frac{2K_2k_4}{K_1K_{10}k_{11}}\right)^{1/2} \frac{P_{\text{CO}_2}{}^{1/2}}{P_{\text{H}_2}{}^{1/2}} + \left(\frac{K_1K_2K_{10}k_{11}}{2k_4}\right)^{1/2} P_{\text{CO}_2}{}^{1/2}P_{\text{H}_2}{}^{1/2} + \frac{P_{\text{CO}}}{K_3}\right)^2}. \quad \text{(A-19)}$$

ACKNOWLEDGMENT

The authors gratefully acknowledge support from the National Science Foundation (Grant No. CPE-7910823).

REFERENCES

1. Vlasenko, V. M., and Yuzefovich, G. E., *Russ. Chem. Rev.* **38,** 728 (1969).
2. Mills, G. A., and Steffgen, F. W., *Catal. Rev.* **8,** 159 (1973).
3. Vannice, M. A., *Catal. Rev. Sci. Eng.* **14,** 153 (1976).
4. "Advances in Fischer–Tropsch Chemistry," ACS Division of Petroleum Chemistry Preprints, Vol. 23, No. 2, 1979.
5. Ponec, V., *Catal. Rev. Sci. Eng.* **18,** 151 (1978).
6. Sughrue, E. L., and Bartholomew, C. H., *Appl. Catal.* **2,** 239 (1982).
7. Binder, G. C., and White, R. R., *Chem. Eng. Prog.* **46,** 563 (1950).
8. Binder, G. C., and White, R. R., Amer. Documentation Inst., Washington, Document 2834.
9. Dew, J. N., White, R. R., and Sliepcevich, C. M., *Ind. Eng. Chem.* **47,** 140 (1955).
10. Dew, J. N., Ph.D. Dissertation, University of Michigan (1953).

11. Nicolai, J., d'Hont, M., and Jungers, J. C., *Bull. Soc. Chem. Belg.* **55,** 160 (1946).
12. Sols, E., *Coll. Chem. Commun. Czech.* **27,** 2621 (1962).
13. Solc, M., and Pour, V., *Coll. Chem. Commun. Czech.* **29,** 857 (1964).
14. Herwijnen, T. V., Van Doesburg, H., and de Jong, W. A., *J. Catal.* **28,** 391 (1973).
15. Lee, C. B., and Anderson, R. B., Private Communication, Sept., 1979.
16. Dalmon, J. A., and Martin, G. A., *JCS Faraday Trans. I* **75,** 1011 (1979).
17. Falconer, J. L., and Zagli, A. E., *J. Catal.* **62,** 280 (1980).
18. Weatherbee, G. D., and Bartholomew, C. H., *J. Catal.* **68,** 67 (1981).
19. Bartholomew, C. H., and Pannell, R. B., *J. Catal.* **65,** 390 (1980).
20. Cratty, L. E., Jr., and Russell, W. W., *J. Amer. Chem. Soc.* **80,** 767 (1958).
21. Bahr, H. A., *Ges. Abhandl. Kenntis Kohle* **8,** 219 (1929).
22. McCarty, J. G., Falconer, J. L., and Madix, R. J., *J. Catal.* **30,** 235 (1973).
23. McCarty, J. G., and Wise, H., *J. Catal.* **57,** 406 (1979).
24. Zagli, A. E., Falconer, J. L., and Keenan, C. A., *J. Catal.* **56,** 453 (1979).
25. Araki, M., and Ponec, V., *J. Catal.* **44,** 439 (1976).
26. Gardner, D. C., and Bartholomew, C. H., *I. & E. C. Fund.* **20,** 229 (1981).
27. Goodman, D. W., Kelley, R. D., Madey, T. E., and White, J. M., *J. Catal.* **64,** 479 (1980).
28. Gardner, D. C., and Bartholomew, C. H., *I. & E. C. Prod. Res. Develop.* **20,** 80 (1981).
29. Bartholomew, C. H., *Catal. Rev. Sci. Eng.* **24,** 67 (1982).
30. Clark, A. C., "The Theory of Adsorption and Catalysis." Academic Press, New York, 1970.
31. Carberry, J. J., "Chemical and Catalytic Reaction Engineering." McGraw–Hill, New York, 1976.
32. Satterfield, C. N., "Heterogeneous Catalysis in Practice." McGraw–Hill, New York, 1980.
33. Weller, S. W., *Adv. Chem. Ser.* **148,** 26 (1975).
34. Biloen, P., Helle, J. N., and Sachtler, W. M. H., *J. Catal.* **58,** 95 (1979).